Research Square

Preprints are preliminary reports that have not undergone peer review.
They should not be considered conclusive, used to inform clinical practice,
or referenced by the media as validated information.

Improvement in stamping formability of Ti/Al multilayered composites via annealing-induced interface modification

Miao Cao

2022009@tyust.edu.cn

Taiyuan University of Science and Technology

Dazhou Wang

Taiyuan University of Science and Technology

Kunkun Deng

Taiyuan University of Technology

Haojie Wang

Taiyuan University of Science and Technology

Pengpeng Xue

Chunbo Zhao

Research Article

Keywords:

Posted Date: November 13th, 2026

DOI: https://doi.org/10.21203/rs.3.rs-11450840/v1

License: This work is licensed under a Creative Commons Attribution 4.0 International License.
Read Full License

Additional Declarations: No competing interests reported.

Improvement in stamping formability of Ti/Al multilayered composites via annealing-induced interface modification

Cao Miao[1, 2], Wang Dazhou[1, 2], Deng kunkun[3*], Wang Haojie[1, 2],Xue Pengpeng[4], Zhao Chunbo[5]

[1] College of Materials Science and Engineering, Taiyuan University of Science and Technology, Taiyuan 030024, China

[2] Shanxi Technology Innovation Center of Flange Basic Component Forming,Taiyuan 030024, China

[3] College of Materials Science and Engineering, Taiyuan University of Technology, Taiyuan 030024, China

[4] Jinxi Industries Group Co., Ltd., Taiyuan 030024, China

[5] Shanxi Yinguang Huasheng Magnesium Industry Co., Ltd, Yuncheng 044000, China

Corresponding author: Deng kunkun, DKKtyut@163.com; Cao Miao, 2022009@tyust.edu.cn

Abstract

Ti/Al/Ti/Al/Ti layered metal composites (LMCs) were obtained via hot-pressing and hot-rolling, followed by annealing at 550 ℃ for different times to regulate the interface. The effect of Ti/Al interfacial evolution on the mechanical behavior and stamping formability of the LMCs was investigated. As annealing proceeded, the Ti/Al interface bonding strength exhibited a rise followed by a decline, reaching a peak of 8.73 N/mm at an annealing duration of 1 h. The strength of the LMCs decreased, whereas elongation (EL) increased first and then decreased, reaching the maximum of 7.15% after 1 h of annealing, which was closely related to superior interfacial bonding. The enhanced interfacial bonding improved deformation compatibility among adjacent layers, thereby delaying premature failure of the less ductile Al layer and increasing the overall EL. The optimal stamping formability was obtained in the LMCs annealed for 1 h, as the weakened basal texture of the base metal induced a lower yield-to-tensile strength ratio (σ_s/σ_b) and a larger strain hardening exponent (n), endowing the LMCs with a longer uniform plastic deformation and higher strain hardening resistance. During stamping, localized and stable interfacial delamination promoted crack deflection and blunting and contributed to energy dissipation, thereby improving the stamping formability of the LMCs, whereas extensive and unstable wedge-shaped delamination provided a rapid interfacial crack-propagation path and accelerated failure.

Keywords: Ti/Al/Ti/Al/Ti layered metal composites, annealing, interface, mechanical behavior, stamping formability

1. Introduction

The skin materials of hypersonic vehicle are required to withstand extreme service environments, including high temperatures, high-speed aerodynamic erosion, thermo-mechanical coupled loading, and complex corrosive conditions[1]. These extreme conditions impose stringent requirements on material lightweighting, toughness, and long-term service reliability. However, existing aircraft skin materials such as superalloys, intermetallic compounds, carbon-based materials, and ceramics have failed to achieve a desirable balance among lightweight characteristics, high specific strength, high specific stiffness, and the formability of large-scale complex components particular, for large-area skin structures with complex geometries, achieving the low-cost and high-efficiency fabrication of high-performance materials remains a major bottleneck restricting their engineering application[2]. In this context, Ti/Al laminated composite sheets, which integrate the corrosion resistance and high-temperature stability offered by with the lightweight characteristics, favorable plastic deformability, and economic benefits of aluminum alloy[3], have attracted considerable attention as potential structural materials with high specific strength. Therefore, they may offer a new materials-design strategy for hypersonic vehicle skin structures.

Five-layer Ti/Al/Ti/Al/Ti layered metal composites (LMCs) are mainly produced through explosive welding [4], hot-pressing [5], hot-rolling [6]and so on. Nevertheless, each individual process has inherent limitations. Xie et al. [7]reported that explosive welding was feasible for Ti/Al bonding. Nevertheless, the process was highly sensitive to processing parameters, which may induce interfacial defects and unstable bonding. Cao et al. [8]revealed that hot-pressing could enhance Ti/Al interfacial bonding, whereas excessive temperatures promoted the growth of brittle $TiAl_3$ phases, thereby deteriorating the formability. Guo et al. [9]reported that during hot-rolling of the LMCs, the deformation incompatibility between Ti and Al, as well as their tendency to oxidize, often weaken the interfacial bonding strength. Hence, to overcome the shortcomings of a single processing method and further optimize the processing performance of the LMCs, the researchers attempted to use a combined process to prepare the LMCs. The hot-pressing and hot-rolling combined process has gained considerable attention owing to its exceptional technological merits. Firstly, hot-pressing can promote diffusion and the initial metallurgical bonding at the interface [10]. Subsequent hot-rolling further improves the microstructural

homogeneity and deformation compatibility of the composites during plastic deformation. The hybrid processing route allows the LMCs to achieve a well-coordinated combination of strength, ductility, and formability [11].

Current studies on the LMCs have mainly concentrated on fabrication methods, interfacial structural evolution, and fundamental mechanical properties [12, 13], while comparatively few studies have addressed their stamping formability. In particular, the mechanism by which the evolution of the Ti/Al interfacial structure influences the stamping formability [14, 15] of the LMCs remains to be further investigated. The substantial differences between Ti and Al in crystal structure, atomic radius, thermal expansion coefficient and so on hinder the formation of strong. In addition, low-ductility intermetallic compounds (IMCs) [16, 17] tend to form at the Ti/Al interface during thermomechanical processing and subsequent heat treatment , which are generally considered detrimental to the mechanical properties and formability of laminated composites. However, the influence of interfacial reaction layers on the overall forming behavior of Ti/Al LMCs is more complex than simply being beneficial or harmful [18]. A moderate interfacial reaction layer may enhance metallurgical bonding and improve stress transfer between constituent layers, whereas excessive growth of brittle intermetallic compounds can restrict interlayer deformation and promote crack initiation [19]. Therefore, achieving superior stamping formability in the LMCs requires precise control over the interfacial structure. Annealing [20]is an effective strategy for interfacial regulation. The appropriate post-rolling annealing can relieve residual stresses and optimize the microstructure, thereby facilitating subsequent forming of the LMCs. Huang et al. [21]revealed that high-temperature annealing at 600 °C promoted Ti/Al interfacial reaction and crack healing, thereby enhancing interlayer deformation compatibility. Cao et al. [8]further demonstrated that annealing effectively improved the interfacial bonding strength and elongation of the LMCs, facilitating the cooperative plastic deformation during the subsequent forming process. Zhang et al. [22]reported that appropriate heat treatment reduced Ti/Al interfacial defects and improved interfacial bonding strength, thereby significantly enhancing the formability of the composites. The above researches suggested that coordinated deformation of laminated composites could be promoted by tailoring the matrix microstructure and interfacial structure through appropriate annealing treatment. However, Ti/Al laminated composites are subjected to complex multiaxial stress, including tension,

compression, and shear during stamping forming [23]. In stamping forming processes characterized by complex stress states, the evolution laws of interfacial structures and their mechanistic roles are still not well clarified. Therefore, it is essential to elucidate the inherent relationship between the development of interfacial characteristics and the stamping formability of laminated composites [24].

In this study, the LMCs were prepared through hot-pressing followed by hot-rolling before being annealed at 550 °C for varying durations to tailor the interfacial microstructure. The relationship between annealing-induced interfacial evolution, deformation compatibility, and stamping formability was systematically investigated, with particular emphasis on damage development during forming. The findings provide new insights into the relationship between interfacial evolution, deformation compatibility, and stamping formability of the LMCs.

2. Experimental methods

2.1. Preparation of materials

The LMCs were fabricated using TA1 (Ti) and 2024 (Al) sheets with thicknesses of 0.3 and 0.5 mm, respectively. Ti and Al sheets in their initial state were diced into 125 mm × 125 mm squares. As schematically illustrated in Fig. 1, the fabrication procedure involved four steps: (i) Pre-treatment of the surface. Surface sanding was performed on the sheets using sandpaper, followed by ultrasonic cleaning in ethanol. After cleaning, the sheets were aligned in the same orientation and stacked according to the Ti/Al/Ti/Al/Ti sequence, followed by placement in the hot-pressing die. (ii) Hot-pressing. The stacked sheets were hot-pressed at 500 °C under 175 MPa for 1 h. (iii) Hot-rolling. The specimens were rolled at 550 °C for three passes at 20 rpm until a final thickness of 1 mm was achieved. (iv) Annealing. The hot-rolled LMCs were treated by annealing at 550 °C for 0.5 h, 1 h, 1.5 h, and 2 h, followed by natural air cooling.

2.2. Microstructure

The matrix microstructure, interfacial morphology, and fracture characteristics (including tensile and Erichsen cupping tests) of the LMCs were characterized via scanning electron microscopy (SEM) coupled with energy-dispersive spectroscopy (EDS), which was also utilized to determine the elemental distribution and concentrations adjacent to the interfaces. The interfacial phases of the LMCs were characterized by X-ray diffraction

(XRD). The crystallographic features within the interfacial regions were analyzed using electron backscatter diffraction (EBSD).

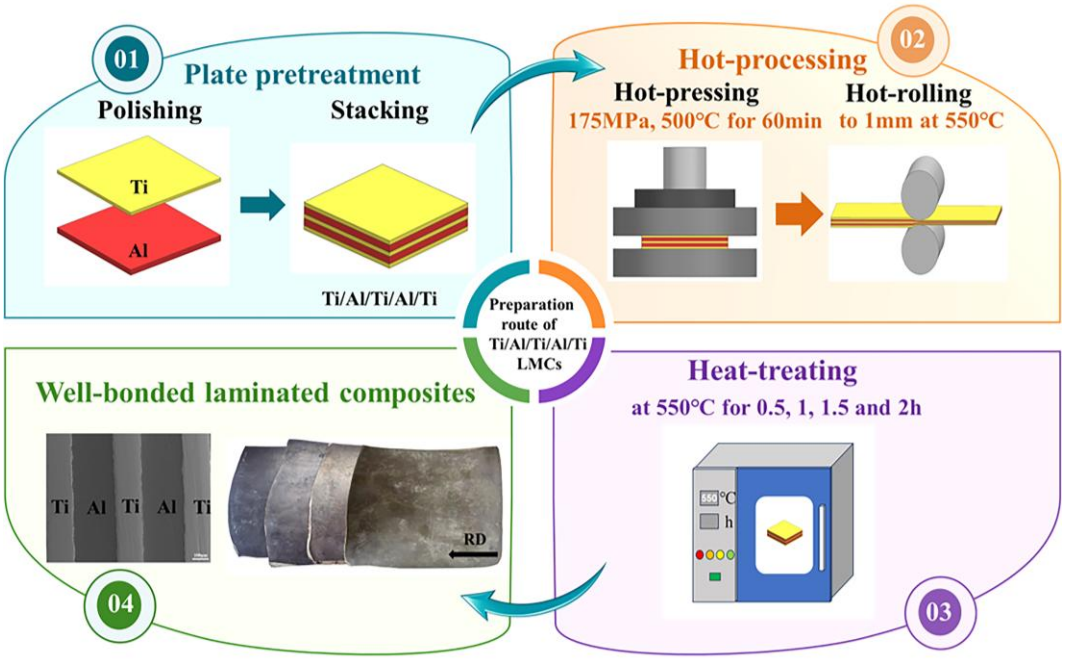


Fig. 1. Schematic diagram of the fabrication process for the LMCs.

2.3. Mechanical properties

The LMCs were sectioned into tensile specimens along the rolling direction (RD), 45° direction, and transverse direction (TD). The tensile tests were performed on an MTS E45.105 universal testing machine with a crosshead speed fixed at 1 mm/min. For each combination of annealing condition and loading direction, at least three independent tensile specimens were tested. The reported tensile properties represent the average values obtained from these independent measurements.

Using an HV-1000 micro-Vickers hardness tester, the Vickers hardness of the constituent metal layers and interfacial regions in the LMCs was evaluated under a 100 gf load for 15 s. Five valid indentations were made at different positions in each constituent layer and interfacial region of each specimen, and the average value was reported as the corresponding Vickers hardness.

The interfacial bonding strength was measured by T-peeling tests according to ASTM D1876-08. The peeling specimens had dimensions of 100 mm × 5 mm (RD × TD). A 30 mm pre-peeled region was introduced using a vice prior to testing, and the tests were

performed at a crosshead speed of 10 mm/min. At least three independent specimens were tested for each annealing condition, and the reported interfacial bonding strengths represent the corresponding average values.

2.4. Stamping formability

The stamping formability of the LMCs was evaluated via Erichsen cupping tests, based on the GB/T 4156-2007 standard. The samples, cut into 55 mm × 55 mm squares (RD × TD), underwent testing with a 20 mm hemispherical punch under a 10 kN blank holder load. At least three independent specimens were tested for each annealing condition. The reported Erichsen indices represent the average values obtained from these independent measurements.

3. Results and discussion

3.1. microstructure

The Ti/Al interfaces of the LMCs subjected to different annealing times were examined by SEM and EDS, with the corresponding results displayed in Fig. 2. As shown in Fig. 2(a), all interfaces exhibit distinct wavy morphologies, indicating that mechanical interlocking was achieved at the interfaces under the rolling force. The EDS mapping results in Fig. 2(b) reveal a narrow and non-uniform interfacial transition zone in the LMCs annealed for 0.5 h, indicating that the interfacial metallurgical reaction is limited and that the interfacial bonding is dominated by mechanical interlocking. This is mainly attributed to the insufficient relief of the high residual stresses generated during hot-rolling, which suppresses atomic interdiffusion across the Ti/Al interface and results in non-uniform elemental diffusion. For the LMCs annealed for 1 h, several small voids can be observed within the interfacial transition zone, as marked by the cyan arrows in Fig. 2(b). These voids are likely to be Kirkendall voids due to the different diffusion rates of Ti and Al atoms [25]. The interfacial transition region becomes markedly wider and more uniform. This can be attributed to the continued annealing, which reduces dislocation density, promotes residual stress relief, alleviates interfacial stress concentration, and enhances elemental interdiffusion across the interface. Therefore, a more uniform bonding is formed in a wider interface region, thereby improving deformation compatibility between the Ti and Al layers. Upon further prolongation of the annealing duration to 1.5 h and 2 h, the interfacial transition zone becomes markedly thicker, as prolonged annealing allows atoms to acquire

sufficient activation energy for diffusion more readily [26]. Meanwhile, some longitudinal and transverse microcracks, voids and local debonding can be observed in the interfacial transition zone, as shown by green, cyan and orange arrows. These features indicate that excessive interfacial reactions may cause local interfacial embrittlement and weaken interfacial bonding. The EDS line-scan results in Fig. 2(c) reveal plateaus at all interfaces. A progressive thickening of the interfacial transition layer is observed with prolonged annealing, reaching 2.53 μm at 0.5 h, 2.91 μm at 1 h, 6.54 μm at 1.5 h, and 11.36 μm at 2 h. These results indicate that the interfacial transition layer gradually thickens with increasing annealing time.

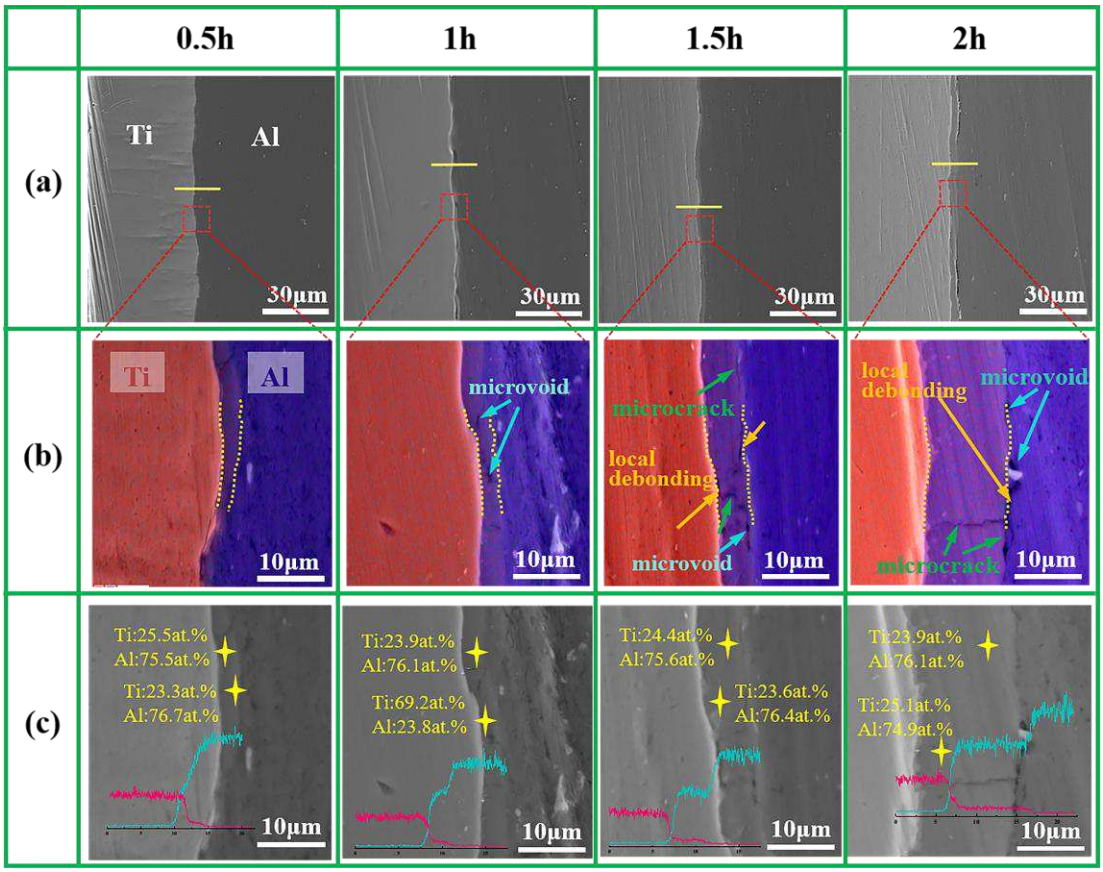


Fig. 2. SEM images and EDS characterization of the Ti/Al interfaces in the LMCs annealed at different times: (a) Ti/Al interfacial morphologies, (b) EDS elemental mapping, and (c) EDS point and line-scan analyses.

Fig. 3 shows the XRD results of the Ti/Al interfaces in the LMCs annealed at different times. Besides the Ti and Al peaks, distinct $TiAl_3$ diffraction peaks are detected. The Ti/Al atomic ratio at the interface is close to 1:3 according to the EDS point analysis in Fig. 2(c),

which, together with the above observations, confirms that $TiAl_3$ is the only detectable intermetallic phase at the Ti/Al interface. A similar conclusion was drawn by Chen et al. [27], who showed that $TiAl_3$ was the only intermetallic phase generated in the Ti/Al interfacial region after annealing at 525–625 °C, as its thermodynamic stability favored preferential nucleation and growth. This regularity aligns with the findings of this work.

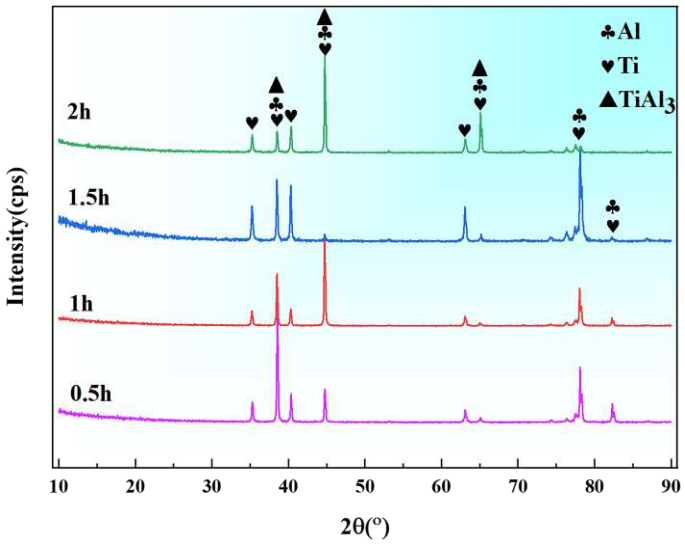


Fig. 3. XRD analysis of the Ti/Al interfaces in the LMCs annealed at different times.

Fig. 4 shows the inverse pole figure (IPF) and pole figure (PF) of the Ti layers in the LMCs annealed at different times. It is evident that the LMCs exhibit a bimodal microstructure, characterized by alternating Ti layers with refined grains and Al layers with relatively coarse grains. PF analysis shows that all Ti layers possess a basal texture with <0001> // ND. The Ti texture intensity values in the LMCs are 6.41, 5.41, 8.92, and 12.23 for annealing times of 0.5 h, 1 h, 1.5 h, and 2 h, respectively. Upon prolonging the annealing time, the Ti texture intensity first decreases and then increases, with the lowest texture observed after annealing for 1 h. After annealing for 0.5 h, recovery dominates the microstructural evolution of the Ti layers, while only partial static recrystallization (SRX) occurs [28], a relatively strong rolling texture is retained. Following 1 h of annealing, the microstructural evolution of the Ti layers gradually shifts from recovery-dominated to recrystallization-dominated behavior, and SRX proceeds more completely. Consequently, a progressive replacement of deformed grains by equiaxed recrystallized grains occurs in the Ti matrix. The resulting random crystallographic orientations reduce the original preferred orientation, thereby promoting texture weakening. However, when the samples

are annealed for 1.5 h and 2 h, grain boundary migration is accelerated. During this process, preferential growth occurs in grains with basal orientations because of their favorable interfacial or strain energy conditions., whereas grains with other orientations are gradually engulfed. Consequently, the basal orientation is re-enhanced, resulting in an increase in basal texture intensity. Therefore, excessive annealing fails to significantly reduce the Ti matrix texture; on the contrary, it enhances the basal texture, which could lead to a decline in the mechanical performance of the LMCs.

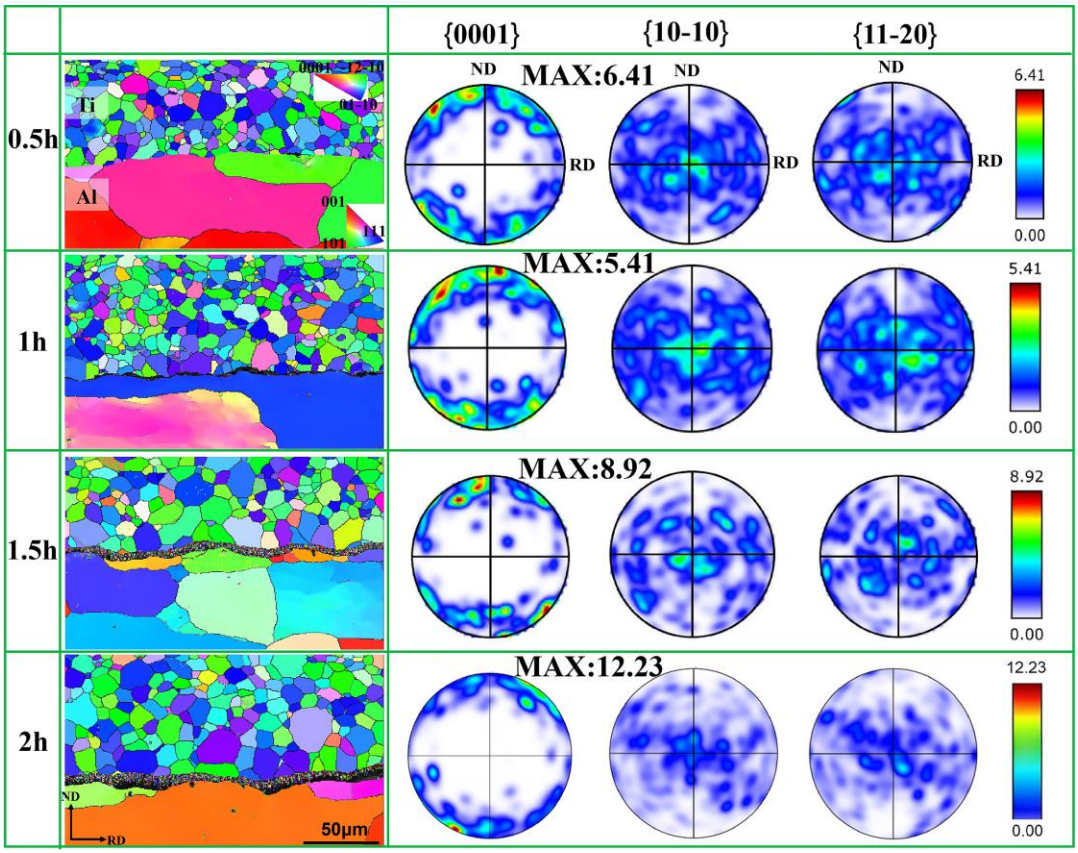


Fig. 4. IPF and PF of the Ti layers in the LMCs annealed at different times.

The distributions of Kernel Average Misorientation (KAM) and Geometrically Necessary Dislocation (GND) within the Ti layers of the LMCs are presented in Fig. 5. For the samples annealed at 0.5 h, 1 h, 1.5 h, and 2 h, the average KAM values are measured to be 0.27, 0.20, 0.24, and 0.21, respectively, whereas the associated ρ_{GND} values correspond to 0.52, 0.36, 0.45, and 0.38 × 10^{14} /m^2. With increasing annealing time, both the KAM value and ρ_{GND} initially decline, followed by a slight rise. The sample annealed for 1 h exhibits the lowest KAM and ρ_{GND} values, indicating that the Ti layer undergoes sufficient recovery and recrystallization at this stage. This reduces the internal stress within

the Ti grains and promotes the relief of accumulated strain. The stored energy accumulated during hot-rolling provides the driving force for microstructural evolution in the Ti layers. After annealing for 0.5 h, static recovery (SRV) dominates the microstructural evolution of the Ti layers, whereas only partial SRX occurs. As a result, relatively high dislocation density and residual stress are retained, leading to relatively high KAM and GND values. Upon increasing the annealing time to 1 h, the Ti layers undergo more complete SRV and SRX, thereby facilitating substantial dislocation annihilation and effective stress release. Consequently, both the KAM and GND values decrease. With further increasing annealing time, the interfacial $TiAl_3$ phase grows rapidly. Owing to its high strength, low ductility, and large crystallographic mismatch with the adjacent Ti matrix, the $TiAl_3$ phase can induce high interfacial stresses and weaken the coordinated deformation capability of the LMCs. This interfacial deformation incompatibility hinders dislocation transfer across the interface, intensifies dislocation entanglement and pile-up, thus causes the KAM and GND values to increase slightly.

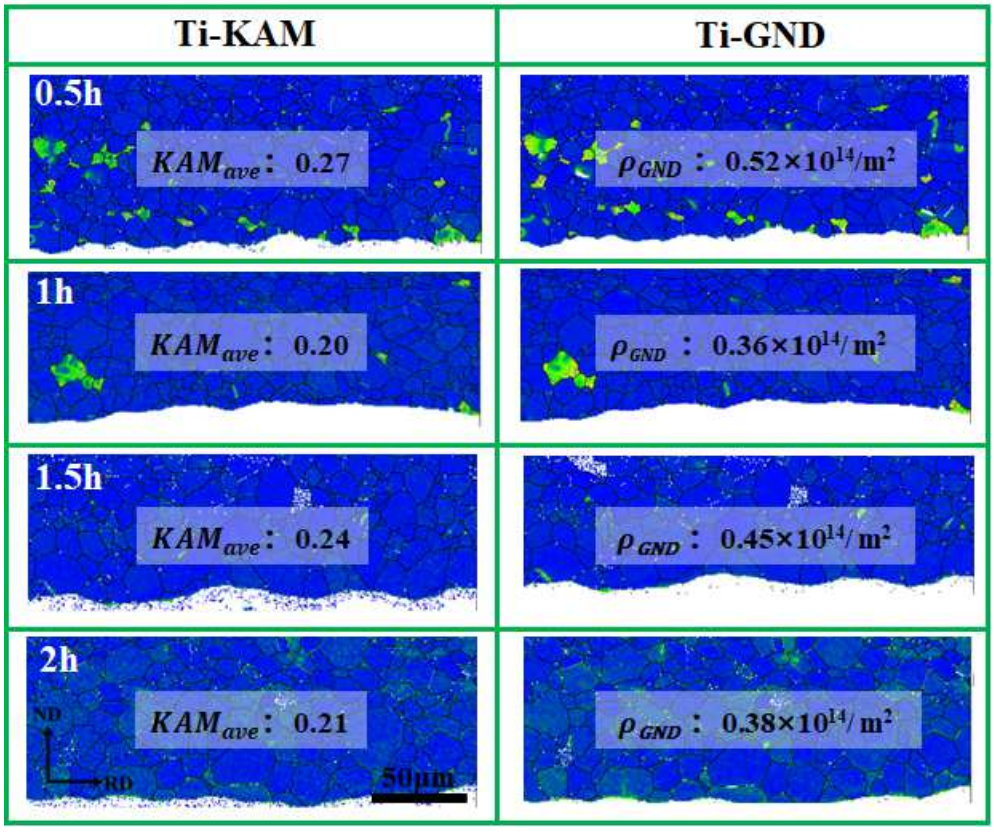


Fig. 5. KAM and GND maps obtained from the Ti layers of the LMCs annealed at different times.

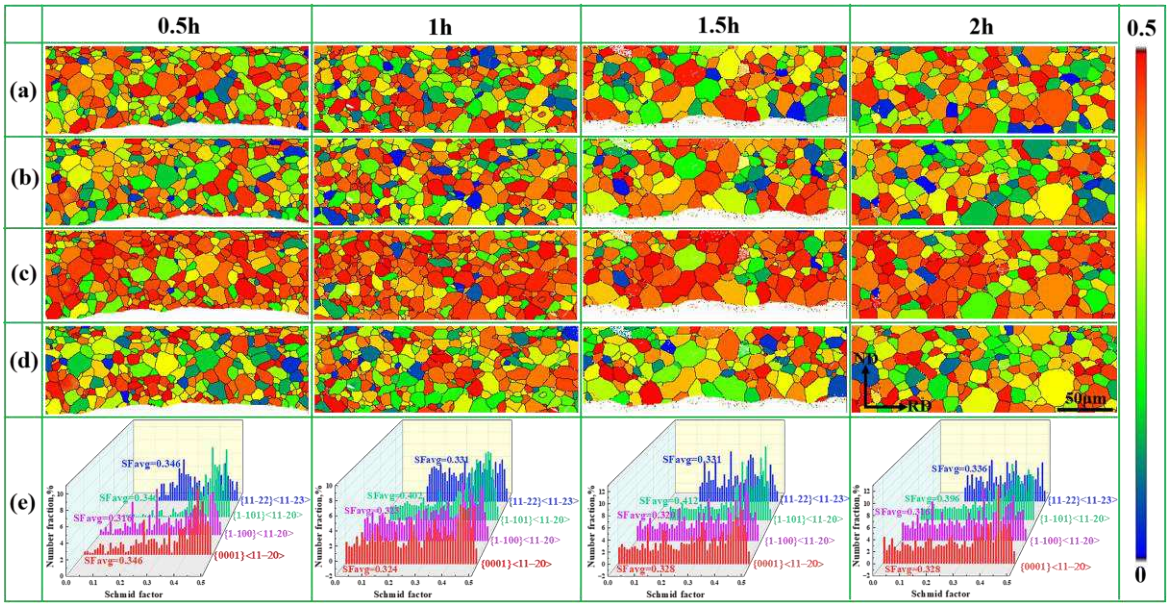


Fig. 6. SF maps of the Ti layer in the LMCs annealed at different times for the (a) {0001}<11-20>, (b) {1-100}<11-20>, (c) {1-101}<11-20>, and (d) {11-22}<11-23> slip systems, and (e) the average SF values.

Fig. 6 shows the Schmid factor (SF) maps and average SF values of the [29]<11-20>, {1-100} <11-20>, {1-101}<11-20>, and {11-22}<11-23> slip systems of the Ti layers in the LMCs annealed at different times. The average SF values of the basal slip system {0001}<11-20> in the LMCs annealed for 0.5 h, 1 h, 1.5 h, and 2 h are 0.346, 0.324, 0.328, and 0.328, respectively, while those of the pyramidal <a+c> slip system {11-22}<11-23> are 0.346, 0.331, 0.331, and 0.336, respectively. For the LMCs annealed for 1 h, the relatively low SF values of the basal and pyramidal <a+c> slip systems indicate that the Ti grains are mainly in hard orientations. Consequently, these slip systems are less readily activated and play a reduced role in plastic deformation. By contrast, the average SF values of the prismatic slip system {1-100}<11-20> in the LMCs annealed for 0.5 h, 1 h, 1.5 h, and 2 h are 0.316, 0.323, 0.320, and 0.316, respectively. The average SF values of the pyramidal <a> slip system {1-101}<11-20> are correspondingly 0.346, 0.402, 0.412, and 0.396, respectively. The prismatic {1-100}<11-20> and pyramidal <a> slip systems {1-101}<11-20> show higher average SF values in the LMCs after 1 h of annealing. This can be attributed to the fact that the Ti layers exhibit the highest degree of SRX after annealing for 1 h, which promotes grain-orientation randomization. Consequently, the geometrical favorability of the prismatic {1-100}<11-20> and pyramidal <a> slip systems {1-101}<11-

20> is enhanced, resulting in higher average SF values. These slip systems are more favorably oriented for activation; therefore, the same applied stress generates a higher resolved shear stress, which makes it easier to exceed the critical value needed to activate slip systems. Meanwhile, the reduction in dislocation density during recrystallization lowers the resistance to slip, thereby enhancing the plastic accommodation capability of the Ti layers and potentially contributing to the improved macroscopic deformation compatibility of the LMCs.

3.2 Mechanical properties

3.2.1 Interfacial bonding strength

Fig. 7 shows the T-peeling test for the LMCs annealed at different time. During the initial peeling stage, the interface remains bonded, and the peeling strength–distance curve increases sharply due to elastic deformation of the matrix metals. Once the curve reaches its peak, it decreases abruptly, indicating that the applied tensile load exceeds the interfacial peeling resistance and triggers interfacial delamination. Thereafter, with continued peeling, the curve shows relatively stable fluctuations with small amplitudes. The peeling strengths of the LMCs annealed for 0.5 h, 1 h, 1.5 h, and 2 h are 5.20 N/mm, 8.73 N/mm, 7.42 N/mm, and 6.91 N/mm, respectively. The peeling strength of the LMCs exhibits a rise followed by a decline as the annealing time is extended, reaching its highest value after 1 h. After 0.5 h of annealing, the interfacial transition zone remained relatively thin. Meanwhile, the high density of retained dislocations near the interface restricted stress release, thereby weakening the interfacial bonding and leading to a lower peeling strength. After 1 h of annealing, Ti and Al atoms gain sufficient thermal activation to overcome the diffusion energy barrier, thereby enhancing interdiffusion and improving interfacial metallurgical bonding. Ma et al. [30]demonstrated that appropriate annealing promotes interfacial atomic diffusion and facilitates the formation of an intermetallic-compound-enriched region, thereby enhancing interfacial strength. Yang et al. [31]further suggested that an appropriate interlayer can produce a gradient diffusion layer, which can relieve residual stresses caused by the mismatch in thermal expansion coefficients, suppress macroscopic cracking at the interface while also improving interfacial bonding. Upon further prolongation of annealing, the peeling strength gradually decreases. This decrease is associated with the accelerated development of intermetallic compounds within the interfacial region during prolonged annealing. Owing to their high strength, low ductility, and large mismatch in thermal

expansion coefficient with the matrix metals, these intermetallic compounds intensify interfacial stress accumulation and weaken interfacial bonding.

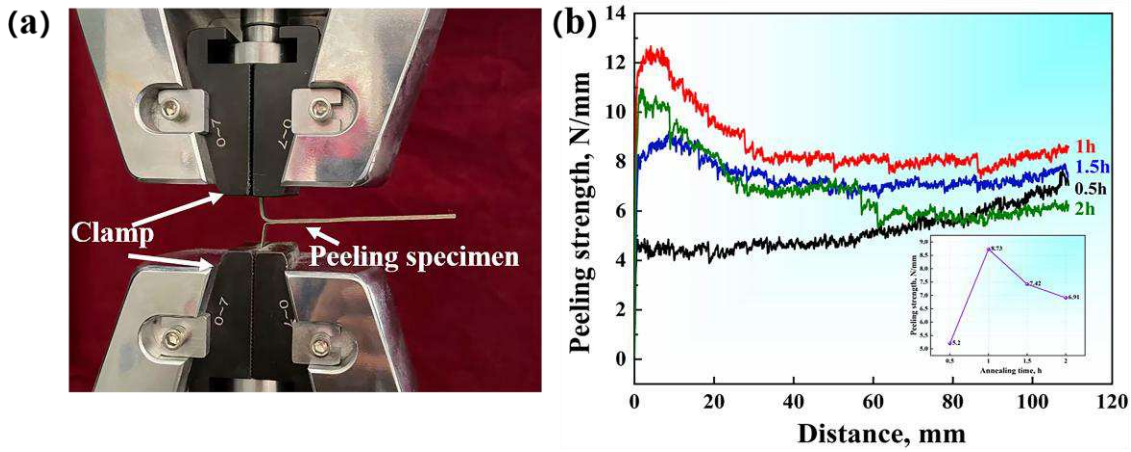


Fig. 7. T-peeling test for the LMCs annealed at different times: (a) T-peeling test device; (b) peeling strength–distance curves and peeling strength change curves.

Fig. 8 shows the SEM and EDS results of the Ti layers in the LMCs after T-peeling tests shown at different annealing times. After 0.5 h of annealing, the Ti surface exhibited only slight Al adhesion, suggesting a limited metallurgical effect on Ti/Al bonding, while mechanical interlocking remained the dominant bonding mechanism. The enlarged view of Fig. 8(a) reveals a few “ridges” and microcracks on the Ti surface, as marked by the gold and pink arrows. EDS point analysis shows that these ridges are mainly Al-rich and are thus denoted as “Al ridges”. The Ti/Al atomic ratio is close to 1:3, confirming the presence of $TiAl_3$ adhered to the Ti surface. These microcracks are likely associated with the ploughing effect of the hard and brittle $TiAl_3$ phase on the Ti surface during T-peeling.. Upon extending the annealing time to 1 h, a thicker interfacial layer was formed due to enhanced Ti–Al interdiffusion, and greater Al retention was observed on the peeled Ti surface. The enlarged view of Fig. 8(b) reveals a higher density of “Al ridges” on the Ti surface, suggesting enhanced Ti–Al interdiffusion and stronger metallurgical bonding. After 1.5 h of annealing, the Ti surface was almost completely covered by Al, while the density of Al ridges decreased noticeably. The enlarged view of Fig. 8(c) reveals numerous densely distributed longitudinal and transverse microcracks on the Ti surface, together with many scattered particulate features, which were confirmed to be $TiAl_3$ particles. This observation indicates that the excessive formation and coarsening of $TiAl_3$ deteriorated the interfacial bonding. Upon further extending the annealing time to 2 h, the Ti surface

exhibited numerous coarse scratches and Al-enriched pits ("Al pits"), as presented in the magnified view of Fig. 8(d). The coarse scratches imply excessive growth of $TiAl_3$, while the non-uniformly sized Al pits indicate discontinuous bonding within the Ti/Al interfacial region. Together, these features are detrimental to interfacial bonding.

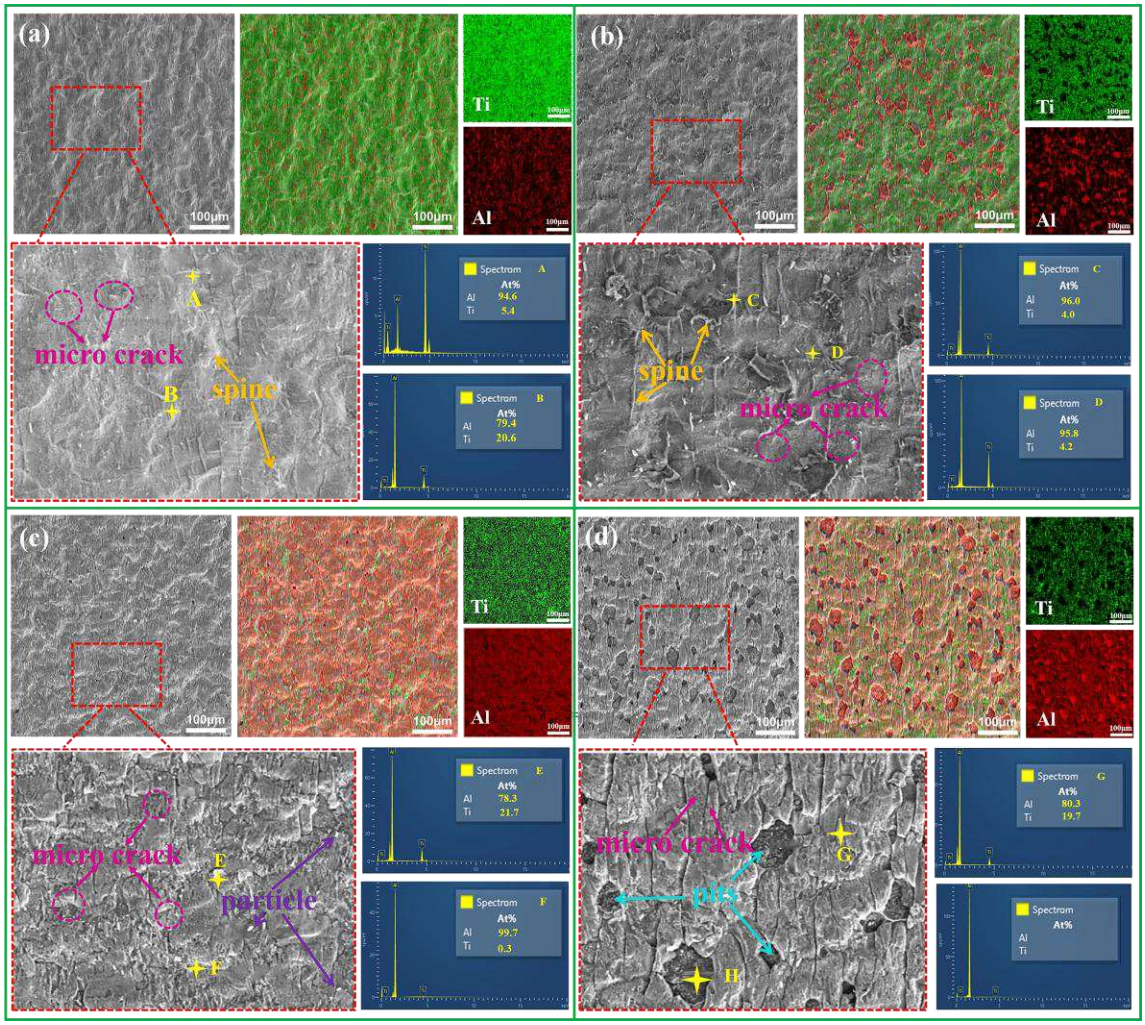


Fig. 8. SEM images and EDS analyses of the Ti layers of the LMCs annealed at different times after T-peeling test: (a) 0.5 h, (b) 1 h, (c) 1.5 h and (d) 2 h.

3.2.2 Microhardness

Fig. 9 presents the Vickers hardness of different layers in the LMCs annealed at different times. The outer Ti layer, inner Ti layer, outer Ti/Al interface, and inner Ti/Al interface are denoted as Ti_1, Ti_2, Ti/Al_1, and Ti/Al_2, respectively. As annealing proceeded, the Ti_1, Ti_2, and Al layers exhibited a continuous decline in hardness. During rolling, the matrix metals accumulated a high density of dislocations and residual stresses. As

annealing proceeded, SRV and SRX occurred to different extents in the matrix metals, leading to extensive dislocation annihilation and thus a gradual decrease in hardness. The Ti_2 layer exhibits slightly higher hardness than the Ti_1 layer, mainly because its internal location subjects it to stronger constraint from the adjacent layers and interfaces. This constraint promotes the accumulation of plastic deformation energy, dislocations, and local residual stress during rolling, thereby resulting in slightly higher hardness than that of the Ti_1 layer. By contrast, the outer Ti_1 layer, directly contacting the rolls, may experience relatively easier stress relief and recovery/recrystallization during annealing, resulting in more pronounced softening.

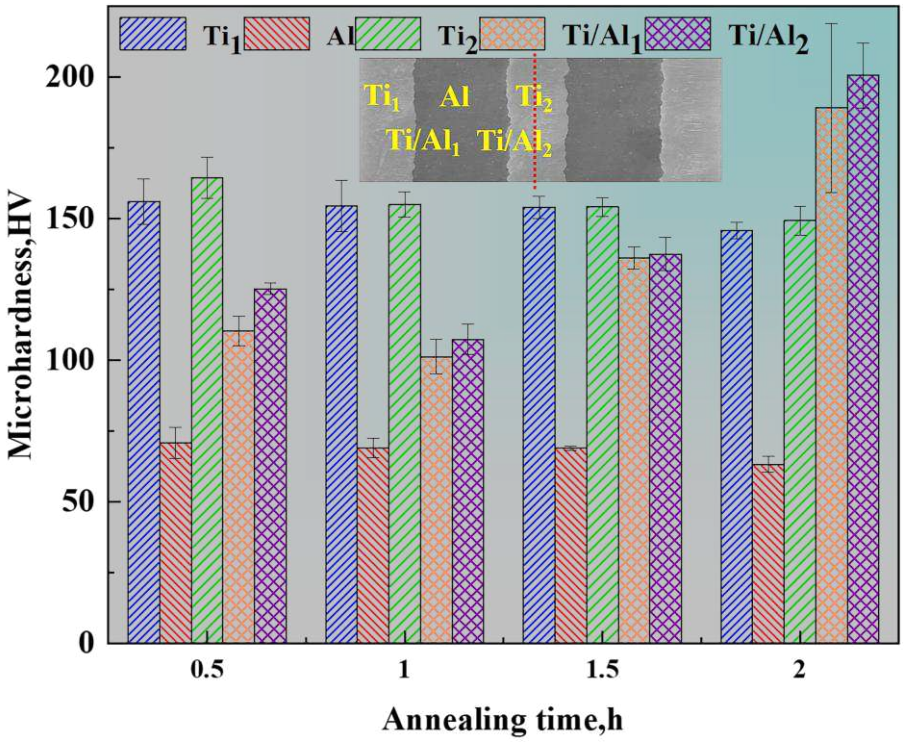


Fig.9. Vickers hardness values of different layers in the LMCs.

Upon extending the annealing time, the Ti/Al interfacial hardness exhibited an initial decline and a subsequent increase, with the lowest value observed in the LMCs annealed for 1 h. For the LMCs after 0.5 h of annealing, the $TiAl_3$ layer formed at the interface was relatively thin. Thus, the relatively high interfacial hardness primarily resulted from the greater hardness of the adjacent matrix metals. After 1 h of annealing, the high-hardness $TiAl_3$ layer at the interface became slightly thicker, but its growth remained limited. Thus, the reduction in interfacial hardness was mainly attributed to recovery and recrystallization

of the matrix metals, together with interfacial residual stress relief. With further extension of the annealing time, the interfacial hardness gradually increased, which was associated with the significant thickening of the interfacial layers, including both the solid-solution and intermetallic regions. The existence of a $TiAl_3$ interfacial phase layer with very high hardness is confirmed by XRD analysis in Fig. 3. Notably, the Ti/Al_2 interface generally shows a modest increase in hardness compared with the Ti/Al_1 interface. The observed difference is likely associated with the slower heat dissipation occurring at the inner Ti/A_l interface during rolling and annealing. The relatively higher thermal stability promotes more active atomic diffusion, thereby inducing limited thickening of the solid-solution and intermetallic layers within the inner interfacial region. Consequently, a modest increase in hardness is observed at the Ti/Al_2 interface compared with the Ti/Al_1 interface.

3.2.3 Tensile properties

The engineering stress–strain curves of the LMCs subjected to different annealing times and tensile-tested along the RD, 45°, and TD orientations are presented in Fig. 10. The corresponding mechanical properties, including yield strength (YS), ultimate tensile strength (UTS), and elongation (EL) to fracture, are summarized in Table 1. The average YS of the LMCs annealed for 0.5, 1, 1.5, and 2 h decreased from 238.91 to 186.89 MPa, with values of 238.91, 205.27, 204.13, and 186.89 MPa, respectively. The corresponding average UTS values were 348.99, 305.99, 303.83, and 278.82 MPa, whereas the average EL values were 6.63%, 7.15%, 6.93%, and 4.79%, respectively. With increasing annealing time, the average YS and UTS gradually decreased, whereas the average EL first increased and then decreased, reaching its maximum after annealing for 1 h. The reduction in YS and UTS was primarily attributed to high-temperature matrix softening mechanisms, such as SRV and SRX, which reduced the dislocation density [32], together with the coarsening of second-phase particles [33]. Chang et al. [34]demonstrated that the reduction in strength of Ti matrix composites at elevated temperatures mainly resulted from matrix thermal softening and increased dislocation mobility. Meanwhile, the coarsening of second-phase particles weakens their impediment to dislocation motion, further reducing the strengthening effect. In contrast, the initial increase and subsequent decrease in EL were mainly governed by the combined effects of matrix softening and Ti/Al interfacial bonding strength. After 1 h of annealing, the enhanced Ti/Al interfacial bonding facilitated effective

stress transfer and strain partitioning between adjacent layers, allowing the Ti and Al constituents to deform more compatibly. Consequently, the onset of necking and subsequent fracture in the less ductile Al layer was delayed, contributing to the increased overall EL of the LMCs [35]. As annealing proceeded beyond 1 h, the reduction in EL of the LMCs was mainly associated with the increased thickness and continuity of the brittle $TiAl_3$ interfacial layer [36]. Upon extending the annealing time, the $TiAl_3$ layer became markedly thicker. Because of its high elastic anisotropy and limited slip activity, the $TiAl_3$ phase has poor deformation compatibility with the matrix metals, which promotes interfacial stress concentration and crack initiation. This leads to premature fracture of the LMCs and thus a reduced EL.

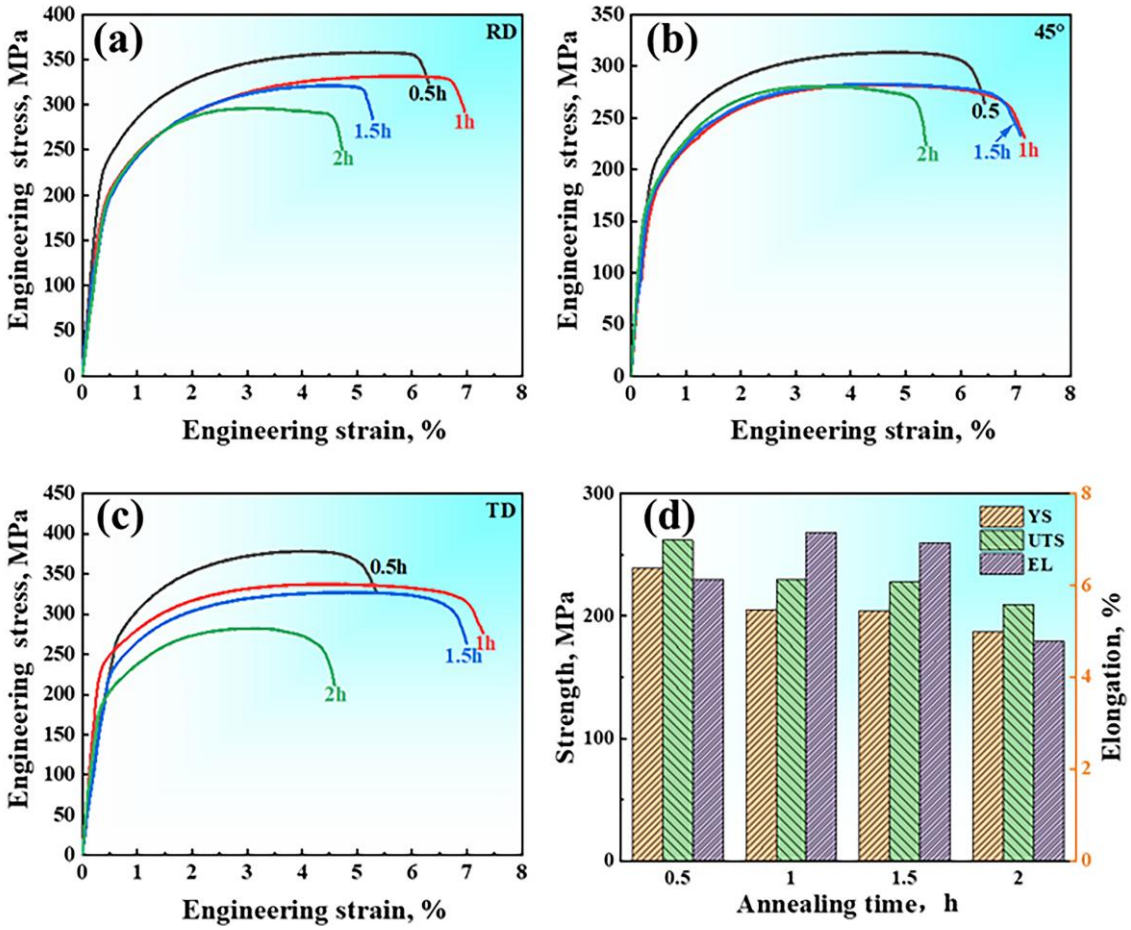


Fig. 10. Engineering stress–strain curves and corresponding mechanical properties of the LMCs annealed at different times: (a) RD, (b) 45°, (c) TD, and (d) YS, UTS, and EL.

Table 1 Mechanical properties of the LMCs annealed at different times along the RD, 45°, and TD.

Annealing Time	Direction	YS/MPa	The average YS/MPa	IPA/%	UTS/MPa	The average UTS/MPa	IPA/%	EL/%	The average EL/%	IPA/%
	RD	231.11±20.31			350.48±10.91			6.30±0.64		
0.5h	45°	224.09±7.80	238.91	17.63	315.10±9.08	348.99	19.87	6.43±0.56	6.63	13.40
	TD	276.33±9.42			415.29±13.33			7.35±1.19		
	RD	221.53±9.75			333.49±5.30			6.96±1.28		
1h	45°	185.06±3.00	205.27	11.40	283.25±1.37	305.99	8.96	7.16±0.29	7.15	3.29
	TD	229.44±8.53			323.98±11.79			7.30±0.60		
	RD	196.72±13.19			320.36±1.95			4.98±0.51		
1.5h	45°	190.01±5.92	204.13	19.36	279.94±17.83	303.83	10.43	7.35±0.28	6.93	23.32
	TD	239.78±10.29			335.09±11.89			8.04±0.92		
	RD	188.27±9.55			269.56±5.18			4.15±0.54		
2h	45°	182.69±11.33	186.89	4.34	285.18±7.56	278.82	4.46	5.10±0.29	4.79	12.35
	TD	193.89±15.22			275.35±6.48			4.79±0.26		

The in-plane anisotropy index (IPA) was introduced to quantify the differences in the mechanical properties of the LMCs along different in-plane directions [8]:

$$IPA=\frac{2\times X_{max}-X_{mid}-X_{min}}{2\times X_{max}}\times 100\% \quad (1)$$

Here, X_{max}, X_{mid}, and X_{min} denote the highest, intermediate, and lowest values, respectively, of a selected mechanical property of the LMCs measured along different directions, such as YS, UTS, or EL. As shown in Table 1, the IPA values of YS for the LMCs annealed for 0.5, 1, 1.5, and 2 h were 17.63%, 11.40%, 19.36%, and 4.34%, respectively. The corresponding IPA values of UTS were 19.87%, 8.96%, 10.43%, and 4.46%, while those of EL were 13.40%, 3.29%, 23.32%, and 12.35%, respectively. The variation in the IPA values indicates that appropriate annealing can effectively weaken mechanical anisotropy and improve in-plane deformation uniformity. During rolling, the LMCs underwent substantial plastic deformation, which resulted in the generation of numerous dislocations and the buildup of residual stresses. After short-term annealing for 0.5 h, incomplete SRX allowed a large fraction of the deformation texture to remain, resulting in pronounced anisotropy in the LMCs. Upon increasing the annealing time to 1 h, more

complete recrystallization weakened the rolling texture and dispersed the grain-orientation distribution, thereby reducing the in-plane anisotropy and lowering the IPA values. Similar studies on laminated composites have reported that annealing-induced recrystallization can weaken the strong deformation texture, reduce the dislocation density. These microstructural changes enhance the ease of slip-system activation under various loading orientations, thereby mitigating mechanical anisotropy [37]. Upon reaching an annealing duration of 1.5 h, grain growth occurred in some orientations, while the Ti/Al interfacial layer thickened and the interfacial brittleness increased, resulting in enhanced anisotropy. Upon annealing to 2 h, the IPA values of UTS and YS decreased again, whereas the IPA value of EL remained higher than that at 1 h. The changes in anisotropy of the LMCs were jointly controlled by texture evolution, grain growth, and interfacial state, rather than being determined by any single factor.

Fig. 11 illustrates the work-hardening rate–true strain (θ–ε) curves of the LMCs annealed for various durations and tested along the RD, 45°, and TD directions. For all LMCs, the θ values gradually decreased as strain increased, reflecting a typical deformation behavior governed primarily by dislocation slip in metallic materials. After short-term annealing for 0.5 h, the high dislocation density and residual stress introduced by rolling were not sufficiently released, and the rolling-induced deformation texture was largely retained. Consequently, the LMCs retained a high initial work-hardening state but had limited further hardening capacity, causing θ to decrease rapidly at the early deformation stage and leading to fracture at relatively low strain. Compared with the other specimens, the LMCs annealed for 1 h showed a higher and more stable work-hardening rate, accompanied by the slowest decrease in θ. This phenomenon is mainly attributed to sufficient recovery and recrystallization, which effectively relieved residual stress and weakened the deformation texture. These changes enhanced the sustained work-hardening capacity of the LMCs and suppressed premature necking [35], ultimately resulting in improved ductility. After 1.5 h of annealing, abundant brittle $TiAl_3$ intermetallic compounds formed at the interface, serving as potential crack-initiation sites and obstacles to dislocation motion. This caused a sharp decay in θ and a significant reduction in fracture strain. After annealing for 2 h, excessive grain growth further reduced the dislocation multiplication capacity, thereby weakening the work-hardening ability and accelerating the onset of plastic instability.

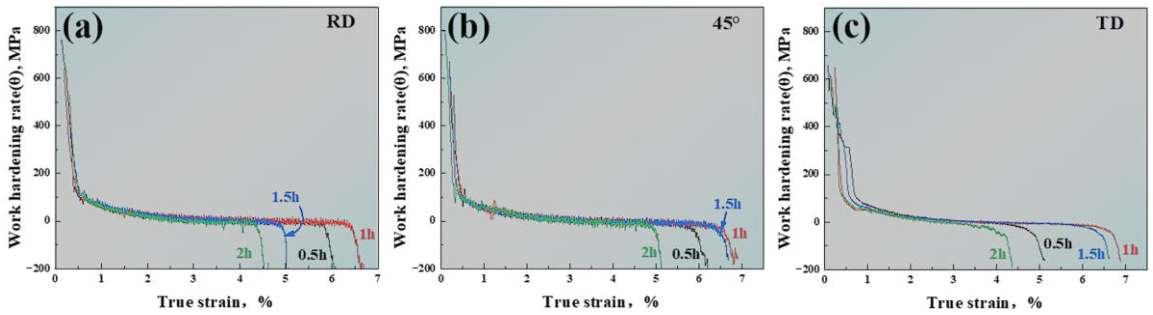


Fig. 11. Work-hardening rate–true strain (θ-ε) curves of the LMCs annealed at different times along (a) RD, (b) 45°, and (c) TD.

The tensile fracture surfaces of the LMCs subjected to different annealing times were examined by SEM, as shown in Fig. 12. As indicated by the cyan and yellow arrows, fracture was accompanied by interlayer separation and necking of the individual layers. The LMCs exhibited interfacial debonding to varying degrees, suggesting that interfacial debonding played a dominant role in the fracture process during deformation process. This behavior primarily arises from the mechanical mismatch between Ti and Al, which results in constraint-induced strain across the Ti/Al boundary and consequently facilitates separation at the interface. In addition, the deformation incompatibility arising from the different necking behaviors of the Ti and Al layers along the ND direction results in localized stress accumulation near the interface. Once the applied normal stress at the Ti/Al interface exceeds the corresponding interfacial bonding strength, severe delamination is triggered. Moreover, the $TiAl_3$ phase generated within the interfacial region further aggravates interfacial debonding. During tensile deformation, cracks preferentially initiated within the Ti/Al interfacial region and extended along the Al layer, thereby inducing fracture initiation in this layer of the LMCs. Numerous dimples were observed across the Ti and Al constituents, confirming that ductile fracture dominated the fracture process. After 0.5 h of annealing, relatively large dimples with an uneven distribution appeared within the Al constituent. After 1 h of annealing, the dimples became smaller, deeper, and more densely and uniformly distributed, reflecting enhanced plastic deformability of the Al matrix; however, with further prolongation of annealing, the Al layer showed fewer dimples, accompanied by larger dimple sizes and a more uneven distribution, implying a deterioration in Al matrix plasticity, in agreement with the reduced EL. The greatest ability to resist plastic instability was achieved in the LMCs after 1 h of

annealing, in line with the observed correlation between microscopic fracture morphology and macroscopic mechanical properties.

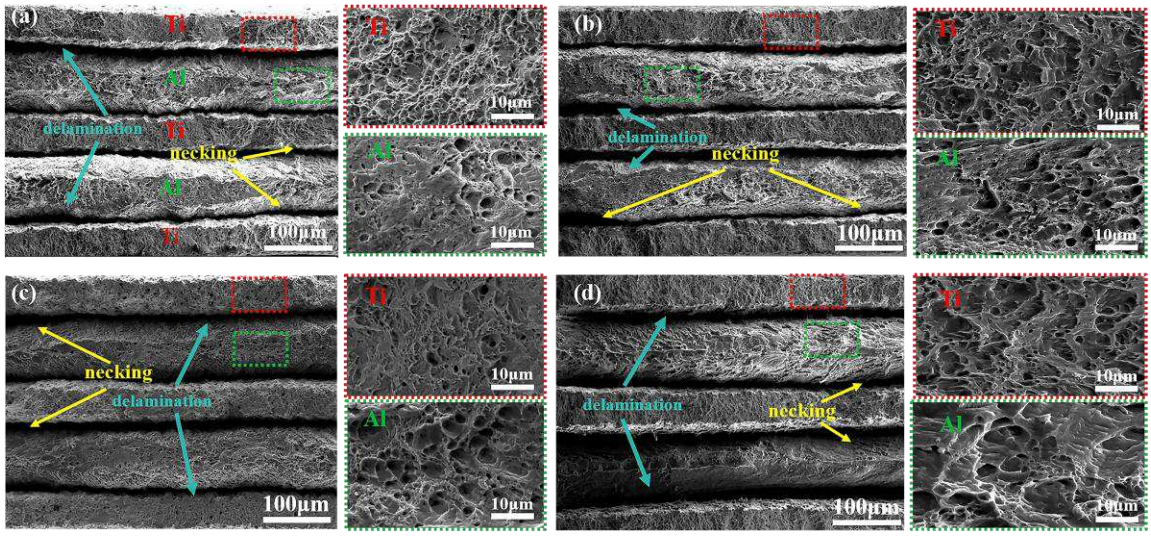


Fig. 12. SEM images of tensile fracture surfaces of the LMCs annealed for (a) 0.5 h, (b) 1 h, (c) 1.5 h, and (d) 2 h.

3.3. Room-temperature forming performance

3.3.1 Formability exponent

The ability of sheet metals to undergo stamping is determined by their work-hardening exponent (n) and yield-to-tensile strength ratio (σ_s/σ_b). Fig. 13 presents the lnσ–lnε curves obtained during the uniform plastic deformation stage, together with the average n and σs/σb values measured along the TD, RD, and 45° directions. The n values were obtained by fitting the lnσ–lnε curves, as shown in Fig. 13(b). Table 2 summarizes the calculated values of these parameters. With the annealing time increased, the n value showed an initial increase and subsequent decrease, with the highest value observed after 1 h of annealing. At this stage, the weakened basal texture of the matrix metals favored plastic deformation through non-basal slip, which contributed to the higher n value. The higher *n* values enhanced the strain-hardening capacity and resistance to localized thinning of the LMCs, thereby delaying the onset of plastic instability (necking) and resulting in enhanced stamping formability of the LMCs. Tian et al. [38] also demonstrated that increasing n is generally associated with reduced yield strength and enhanced elongation, thereby leading to superior formability. Fig. 13(c) presents the average σs/σb ratios of the LMCs annealed at different times. The σ_s/σ_b ratio of the LMCs, subjected to extended annealing, initially

declined before rising again., with the lowest value obtained after annealing for 1 h. This indicates that the LMCs had a relatively extended stage of uniform plastic deformation and could sustain greater plastic strain before failure, thereby improving their formability. This result is consistent with the highest cupping value (IE value) obtained under this annealing condition. Sun et al. [39]demonstrated that a lower σ_s/σ_b ratio suppresses strain localization and delays necking in sheet metals, accompanied by increased elongation and improved sheet-forming capability.

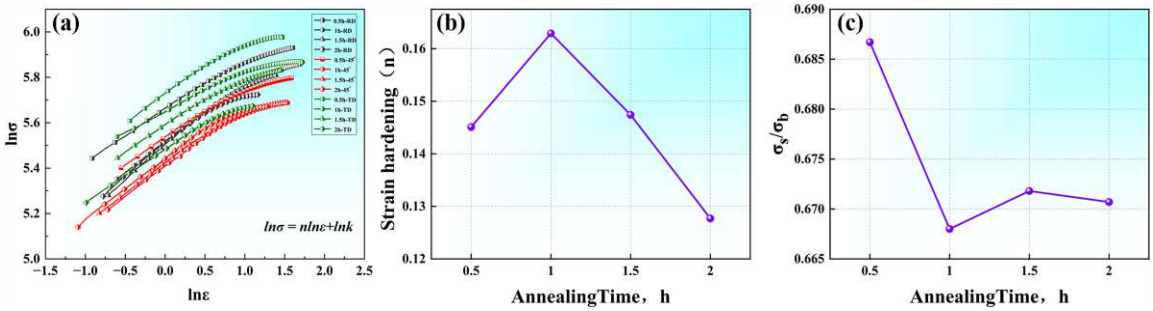


Fig. 13. (a) lnσ–lnε curves during the uniform plastic deformation stage, (b) n values, and (c) σ_s/σ_b variation curves of the LMCs.

Table 2 σ_s/σ_b and n values of the LMCs annealed at different times.

Annealing Time	Direction	σ_s/σ_b	$\overline{\sigma_s/\sigma_b}$	n	$\bar{n}$
0.5h	RD	0.6594	0.6867	0.10181	0.1451
	45°	0.7111		0.15281	
	TD	0.6653		0.17314	
1h	RD	0.6643	0.6680	0.17838	0.1629
	45°	0.6533		0.17586	
	TD	0.7081		0.12149	
1.5h	RD	0.6141	0.6718	0.13352	0.1474
	45°	0.6788		0.15666	
	TD	0.7155		0.14286	
2h	RD	0.6984	0.6707	0.14774	0.1277
	45	0.6406		0.11302	
	TD	0.7030		0.13695	

3.3.2. Formability

The Erichsen cupping performance of the LMCs is governed primarily by the interfacial bonding strength and EL. The Erichsen cupping response of the LMCs is

presented in Fig. 14. The IE values of the LMCs annealed for 0.5, 1, 1.5, and 2 h were 7.46, 7.62, 7.15, and 6.96 mm, respectively. As the annealing time was extended, the IE value of the LMCs exhibited an initial increase before decreasing, with the maximum value observed after 1 h of annealing. This trend corresponds to the LMCs annealed for 1 h, which show enhanced elongation, a reduced σs/σb ratio, and a higher strain-hardening exponent. These results indicate that moderate annealing effectively improves the stamping formability of the LMCs by reducing dislocation density, facilitating the release of residual stresses, and promoting microstructural homogenization through SRV and SRX.

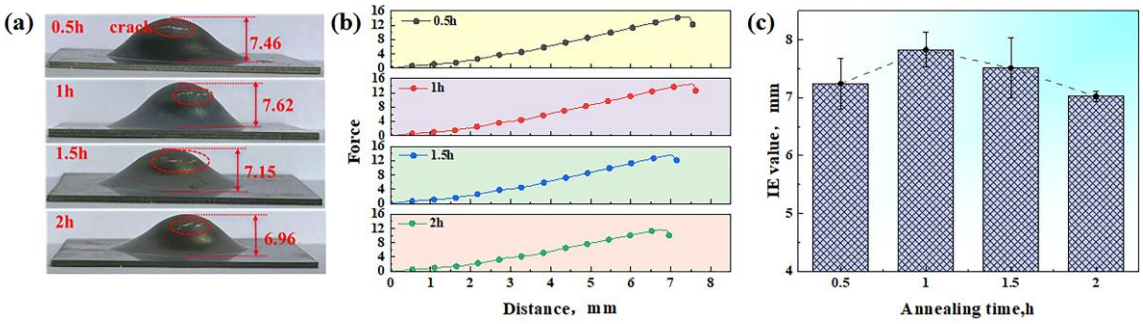


Fig. 14. Erichsen cupping tests of the LMCs: (a) Erichsen cupping specimens and crack morphologies, (b) Force–displacement curves and (c) IE values.

Fig. 15 presents the crack evolution characteristics of the annealed LMCs after cupping deformation. The outer Ti layer experienced the highest strain, and cracks initiated and rapidly propagated to the interface, where different degrees of tearing and deflection occurred, as evidenced by the green and yellow arrows in Fig. 15. The cracks then propagated through the entire LMCs, ultimately leading to failure. In the LMCs annealed for 0.5 h, the relatively weak interfacial bonding resulted in weak constraint between the Ti and Al constituents. During forming, the mismatch in plastic deformation between the Ti and Al constituents generated local internal stresses at the interface, leading to numerous localized debonding sites and micro-delaminations. As the dominant crack reached the Ti/Al interface, part of the stored energy was released through local debonding and micro-delamination. Consequently, further crack propagation required additional energy absorption, thereby delaying failure of the LMCs and leading to relatively good formability. In the LMCs annealed for 1 h, the interfacial bonding

strength was improved. On the one hand, the strong interfacial constraint altered the local stress field near the advancing crack front and enhanced the resistance to further crack growth. On the other hand, severe delamination was not observed at the interface, and only a few localized debonding sites were observed near the crack. When the crack propagated to the interface, a certain degree of tearing and deflection occurred, accompanied by partial dissipation of fracture energy within the interfacial region. These effects prolonged the fracture path and enhanced the resistance to further crack extension, thereby improving the formability of the LMCs. With further prolongation of the annealing time, the excessive formation of brittle $TiAl_3$ along the interfacial region deteriorated interfacial bonding and promoted the generation of numerous voids, microcracks, and severe wedge-shaped delamination, as marked by the cyan, light blue, and orange arrows. Once the dominant crack extended toward the bonding region, it coalesced with the voids or secondary microcracks, thereby accelerating the failure of the LMCs.

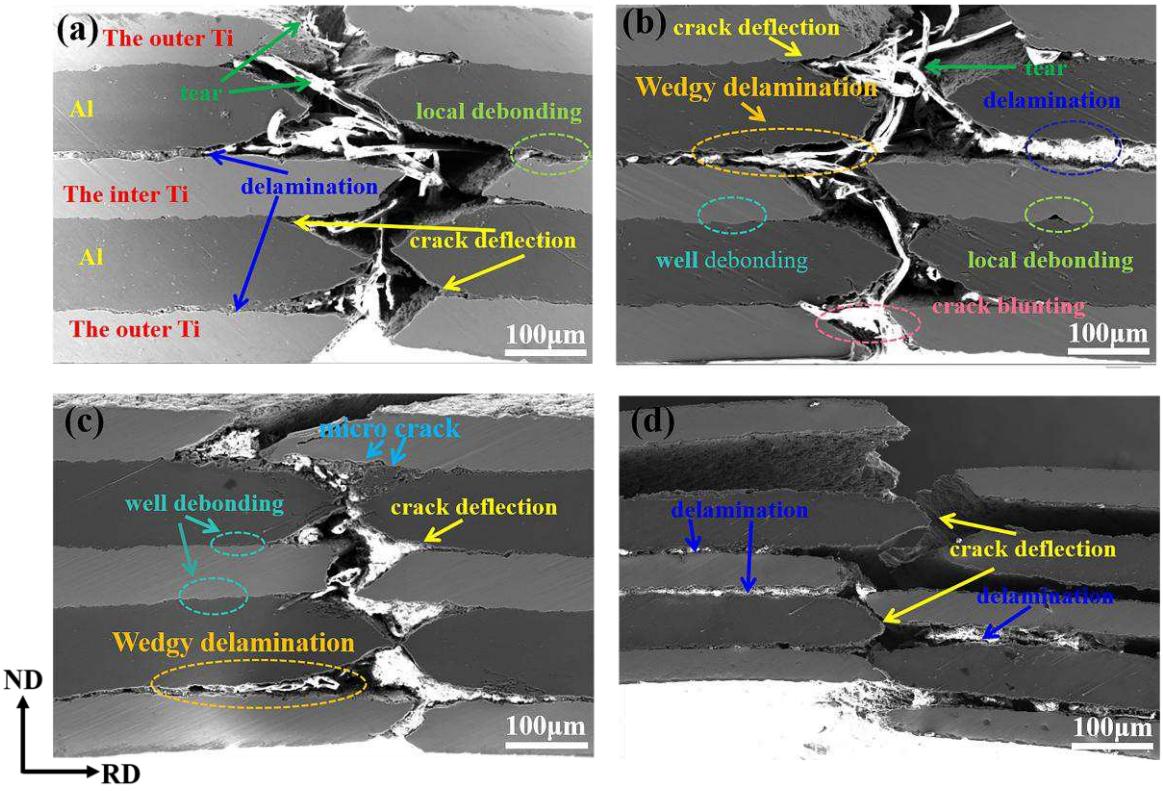


Fig. 15. Erichsen cupping crack propagation morphologies of the LMCs annealed for (a) 0.5 h, (b) 1 h, (c) 1.5 h, and (d) 2 h.

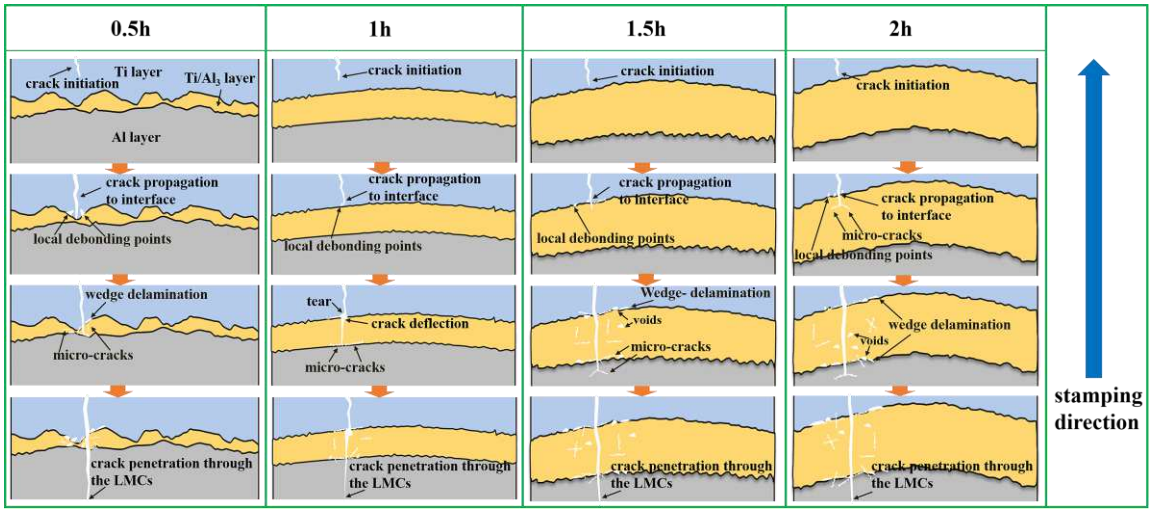


Fig. 16. The schematic of crack propagation of Erichsen cupping specimens.

Fig. 16 presents the schematic of crack propagation of Erichsen cupping specimens. The bonding strength and reaction phases at the Ti/Al interface determine the interfacial stress transfer and strain distribution effects, thereby determining the crack propagation mechanism. For the LMCs annealed for 0.5 h, only a thin and discontinuous $TiAl_3$ layer is present, accompanied by weak metallurgical bonding within the interfacial region. Regions with locally weak bonding readily serve as initiation sites for early-stage interfacial delamination. As the primary crack propagates to the interface, it connects with these localized delamination points, triggering microcrack formation and releasing substantial energy. Consequently, additional energy accumulation is required for further crack propagation, thereby delaying overall LMC failure. After 1 h of annealing, the $TiAl_3$ reaction layer thickens and becomes more uniform, enhancing interfacial diffusion and metallurgical bonding strength. This improved interface constraint effectively suppresses premature interfacial debonding. As the crack approaches the interfacial region, the local stress field at the crack tip is altered by the strong interfacial constraint, resulting in pronounced tearing and deflection of the primary crack. Localized interfacial debonding and secondary microcracks are induced, allowing the energy associated with crack growth to be dissipated and the fracture path to be prolonged, thereby further improving the stamping formability. Boonrang et al. [40]also demonstrated that limited and stable interfacial delamination can promote crack deflection, inhibit rapid crack propagation, and dissipate fracture energy. However, with prolonged annealing, excessive growth of the brittle $TiAl_3$ phase reduces interfacial toughness, promoting the formation of voids,

microcracks, and wedge-shaped interfacial delaminations. As the primary crack reaches the interface, the primary crack readily coalesces with interfacial defects and secondary microcracks, forming pronounced wedge-shaped delaminations that accelerate the forming failure of the LMCs.

4. Conclusion

The LMCs were successfully fabricated through a combined hot-pressing and hot-rolling route, followed by annealing at 550 °C for different durations to regulate the interfacial structure. The role of interfacial microstructural evolution in controlling the tensile behavior and stamping formability of the LMCs was clarified. The main conclusions are summarized below:

(1) Upon prolongation of the annealing time, the Ti layer of the LMCs exhibited an initial reduction followed by an increase in basal texture intensity, reaching its minimum at 1 h. This behavior was attributed to sufficient SRX, resulting in a more randomized grain orientation. The prismatic {1-100}<11-20> and pyramidal <a> {1-101}<11-20> slip systems in the Ti layer of the LMCs annealed for 1 h exhibited relatively high SF values, implying that slip activation on these systems was more favorable. Moreover, the reduced KAM and GND values indicated a lower level of internal residual stress and dislocation accumulation in the LMCs, which provided favorable conditions for plastic deformation.

(2) Excellent interfacial bonding was achieved in the LMCs, accompanied by the formation of micron-scale $TiAl_3$ phases at the interface. As annealing proceeded, the interfacial bonding strength underwent a rise followed by a decline, achieving the maximum of 8.73 N/mm after 1 h of annealing. This was attributed to sufficient atomic interdiffusion across the Ti/Al interface, which formed a strong metallurgical bond. However, prolonged annealing caused excessive growth of IMC, inducing high interfacial stress and deteriorating the interfacial bonding.

(3) The strength of the LMCs experienced a gradual decline as annealing proceeded, whereas EL attained a peak value of 7.15% after 1 h of annealing and subsequently declined. This behavior was primarily related to the matrix recrystallization softening and excellent interfacial bonding strength, which promoted stress transfer and strain redistribution across the Ti/Al interface. These effects effectively delayed necking and fracture of the less ductile Al layer, thereby improving the overall EL of the LMCs.

(4) The optimal stamping formability of the LMCs was obtained after annealing for 1 h, which was influenced by the combined effects of texture intensity and interfacial structure. After 1 h annealing, weakened basal texture resulted in a lower σ_s/σ_b and a larger n value of LMCs, endowing LMCs with longer uniform plastic deformation and higher strain hardening resistance. During stamping, localized and stable interfacial delamination promoted crack deflection and blunting and contributed to energy dissipation, thereby improving the stamping formability of the LMCs, whereas extensive and unstable wedge-shaped delamination provided a rapid interfacial crack-propagation path and accelerated failure.

Acknowledgments

This work was supported financially by the Doctoral research Foundation of Taiyuan University of Science and Technology (Grant.20222081) and the Shanxi Yinguang Huasheng Magnesium Industry Co. (Project Number: 2024350 and C2024039).

Declarations

Conflict of interest The authors declared that they have no conflict of interest to this work.

References

1. Fikry, M. J. M., Arai, Y., Inoue, R., Vinogradov, V., Tan, K. T., Ogihara, S.: Damage Behavior in Unidirectional CFRP Laminates with Ply Discontinuity. Appl. Compos. Mater. 32, 1481 – 99(2025).https://doi.org/10.1007/s10443-025-10320-w
2. He, B., Zheng, X., Yang, Q., Zou, Y., Wu, K., Liu, Z., Gong, J., Li, Z.: Damage Resistance of Honeycomb Sandwich Composites under Low-Energy Impact. Appl. Compos. Mater. 32, 703 – 32(2024).https://doi.org/10.1007/s10443-024-10278-1
3. Mingze, M., Ya, D., Hanyu, L., Huiru, Z.: Failure Analysis of Particle Reinforced Aluminum Matrix Composite With a Microscopic Mechanical Model Using Modified GTN Model. Appl. Compos. Mater. 32, 1835–56(2025).https://doi.org/10.1007/s10443-025-10333-5
4. Pohl, P. M., Brodwolf, R., Ma, D., Göken, M., Höppel, H. W.: Damage tolerant fatigue behavior of laminated metallic composites with dissimilar yield strength. J. Mater. Sci. 60, 939 – 63(2024).https://doi.org/10.1007/s10853-024-10550-6
5. Assari, A. H.: Investigating the deformation behavior of hot-pressed Ti/Al/Ti laminated composite. J. Manuf. Process. 95, 369–81(2023).https://doi.org/10.1016/j.jmapro.2023.04.026
6. Liu, Z., Luo, Z., Zhang, X., Yang, J., Feng, Y., Peng, W.: Study on the microstructure, recrystallization, and mechanical properties of hot-press sintered (TiC + B4C)/6061Al composites during hot rolling. Mater. Charact. 216, 114286(2024).https://doi.org/10.1016/j.matchar.2024.114286
7. Xie, Q., Gao, Y., Qiao, Y., Zhang, Q.: Study on Explosion Welding of Titanium–Aluminum Laminated Plates with Different Explosive Charges. Coatings 14, 1574(2024).https://doi.org/10.3390/coatings14121574
8. Cao, M., Deng, K.-k., Nie, K.-b., Wang, C.-j., Wang, L., Liang, W.: Microstructure, mechanical properties and formability of Ti/Al/Ti laminated composites fabricated by hot-pressing. J. Manuf. Process. 58, 322–34(2020).https://doi.org/10.1016/j.jmapro.2020.08.013
9. Guo, S., Wang, F. R., Wang, Y. Q., Xie, G. M.: Microstructural evolution and properties of Ti/Al clad plate fabricated by vacuum rolling and heat treatment. Mater. Sci. Eng. A 882,

145445(2023).https://doi.org/10.1016/j.msea.2023.145445
10. Liu, S., Sinke, J., Dransfeld, C.: Experimental Characterisation of Cure-Dependent Spring-Back Behaviour of Metal-Composite Laminates in a Hot-Pressing Process. Appl. Compos. Mater. 32, 173–98(2024).https://doi.org/10.1007/s10443-024-10266-5
11. Kamal, S. M., Zani, L., Kadir, A. A., Baxevanakis, K. P., Roy, A.: Advancement and emerging challenges in electric-field assisted manufacturing: a review. Int. J. Adv. Manuf. Technol. 141, 2447 – 70(2025).https://doi.org/10.1007/s00170-025-16499-3
12. Zhao, J., Meng, L., Ya, B., Ren, H., Li, S., Zhou, B.: Effect of layered structural parameter on microstructure and mechanical properties of Ti/Al3Ti laminated composites. Mater. Charact. 230, 115818(2025).https://doi.org/10.1016/j.matchar.2025.115818
13. Zhao, J., Zhang, B., Zhao, T., Zhang, Z., Lei, Z., Wang, Z., Zhang, Z., Zhan, S., Dang, L., Wang, K.: Effects of stacking sequence of the layers on deformation behavior and microstructure evolution of Ti/Ni laminated metal composites. J. Mater. Res. Technol. 34, 2298 – 313(2025).https://doi.org/10.1016/j.jmrt.2024.12.177
14. Zhang, L., Shen, C., Miao, B., Liang, J., Zhao, J., Zhang, J., Dong, Y., Zheng, S.: Microstructural evolution of Zn coating on 22MnB5 steel during austenitization and hot stamping processes. J. Mater. Res. Technol. 37, 2764–73(2025).https://doi.org/10.1016/j.jmrt.2025.06.206
15. Fan, J., Chen, Z., Zhao, D., Liang, X., Zhang, Z., Hu, Z., Zhang, Z., Tang, B., Kou, H., Wang, J., Li, J.: Temperature-dependent crack behavior and microstructure evolution mechanisms in hot stamped Ti65 titanium alloy sheets. J. Alloys Compd. 1037, 182482(2025).https://doi.org/10.1016/j.jallcom.2025.182482
16. Zhang, H., Wang, A., Pan, A., Xie, J., Yang, W.: Effect of intermetallic compound layer thickness on the interface deformation mechanism and mechanical properties of polycrystalline Cu/Al2Cu/Al layered composite materials. Mater. Today Commun. 49, 114297(2025).https://doi.org/10.1016/j.mtcomm.2025.114297
17. He, M., Wang, Q., Wang, J., Ma, N., Wang, Y.: Ultrasonic assistance for fatigue properties improvement of AA6061/Ti6Al4V dissimilar joints by resistance spot welding. CIRP J. Manuf. Sci. Technol. 61, 324–35(2025).https://doi.org/10.1016/j.cirpj.2025.06.004
18. Mohammadi, B., Yousefi, A., Khonsari, M.: Interlaminar Fracture Behavior of Composites: The Role of Interface Layers Angle and Cure State in Mode I Delamination Growth. Appl. Compos. Mater. 33, 2026).https://doi.org/10.1007/s10443-026-10477-y
19. Giannakopoulou, A., Jonsson, M., Costa, S., Saseendran, S., Loukil, M. S.: Effect of Manufacturing Defects on Damage Initiation and Propagation in Gapped UD Carbon Fibre Composite Laminates. Appl. Compos. Mater. 33, 2026).https://doi.org/10.1007/s10443-026-10538-2
20. Liu, J., Weng, Y., Zhou, G., Ju, D., Zhang, J., Lv, Z., Che, L., Wu, Z.: Influence of annealing duration on the microstructure and mechanical properties of CrMnFeCoNi high-entropy alloy fabricated by hot isostatic pressing. J. Alloys Compd. 1048, 185232(2025).https://doi.org/10.1016/j.jallcom.2025.185232
21. Huang, H. G., Chen, P., Ji, C.: Solid-liquid cast-rolling bonding (SLCRB) and annealing of Ti/Al cladding strip. Materials & Design 118, 233–44(2017).https://doi.org/10.1016/j.matdes.2017.01.042
22. Zhang, J., Ma, L., Cai, Z., Zhao, G., Jia, W., Liu, P.: Effect of annealing on the microstructure and mechanical anisotropy of Mg/Al composite plate. J. Magnes. Alloys 12, 5164 – 78(2024).https://doi.org/10.1016/j.jma.2023.12.001
23. Zeng, X., Daniel, C. S., Asheshov, W., Michalik, S., Prangnell, P., Quinta da Fonseca, J.: Effect of Temperature, Strain and Microstructure on Texture Evolution of Ti-6Al-4V During Hot Rolling. Metall. Mater. Trans. A 56, 4620–43(2025).https://doi.org/10.1007/s11661-025-07929-8
24. Jiao, X., Zhang, Y., Wu, Q., Feng, P.: Reaction Process and Evolution Mechanism of Porous Ti–Al–Si Intermetallic Compounds Synthesized by Thermal Explosion. Metall. Mater. Trans. A 56, 1829 – 37(2025).https://doi.org/10.1007/s11661-025-07747-y
25. Huang, Z., Meng, L., Lin, P., Cao, X., Zhang, Z., Liu, G.: Formability improvement of hot-pressed Ti/Al laminated sheet by TiAl3 layer growth and crack healing during deformation. J. Alloys Compd. 938, 168604(2023).https://doi.org/10.1016/j.jallcom.2022.168604
26. Gao, B., Barella, S., You, B., Xiao, H., Yu, C., Liu, C., Gruttadauria, A., Mapelli, C.: Study on the mechanism of synergistic improvement of bonding strength and elongation of Ti/Al composite plates by annealing treatment. Mater. Sci. Eng. A 941,

148603(2025).https://doi.org/10.1016/j.msea.2025.148603
27. Chen, Z., Wang, D., Cao, X., Yang, W., Wang, W.: Influence of multi-pass rolling and subsequent annealing on the interface microstructure and mechanical properties of the explosive welding Mg/Al composite plates. Mater. Sci. Eng. A 723, 97–108(2018).https://doi.org/10.1016/j.msea.2018.03.042
28. Guo, B., Gao, H., Kong, C., Wang, Z., Cui, H., Yu, H.: Transverse texture weakening and anisotropy improvement of Ti-6Al-4V alloy sheet via asymmetric rolling and static recrystallization annealing. J. Alloys Compd. 1010, 177507(2025).https://doi.org/10.1016/j.jallcom.2024.177507
29. Zhou, J., Luo, N., Liang, H., Sun, W.: Multi-scale simulation and microstructure characteristics of TC4 ELI/Al 6013 plates by explosive welding. J. Manuf. Process. 124, 1180 – 92(2024).https://doi.org/10.1016/j.jmapro.2024.07.014
30. Ma, M., Huo, P., Liu, W. C., Wang, G. J., Wang, D. M.: Microstructure and mechanical properties of Al/Ti/Al laminated composites prepared by roll bonding. Mater. Sci. Eng. A 636, 301 – 10(2015).https://doi.org/10.1016/j.msea.2015.03.086
31. Yang, B., Wei, B., Fu, W., Ye, P., Wang, X., Fang, W., Li, X., Li, R., Wu, H., Fan, G.: Effect of interfacial reaction layers on crack propagation behavior of Ti/Al layered metal composites in uniaxial tensile test from the perspective of local strain. Mater. Sci. Eng. A 942, 148669(2025).https://doi.org/10.1016/j.msea.2025.148669
32. Chang, D., Wang, P., Zhao, Y.: Effects of asymmetry and annealing on interfacial microstructure and mechanical properties of Cu/Al laminated composite fabricated by asymmetrical roll bonding. J. Alloys Compd. 815, 152453(2020).https://doi.org/10.1016/j.jallcom.2019.152453
33. Zhang, X., Yu, Y., Liu, B., Zhao, Y., Ren, J., Yan, Y., Cao, R., Chen, J.: Microstructure characteristics and tensile properties of multilayer Al-6061/Ti-TA1 sheets fabricated by accumulative roll bonding. J. Mater. Process. Technol. 275, 116378(2020).https://doi.org/10.1016/j.jmatprotec.2019.116378
34. Chang, S., Du, W., Zhao, Z., Bai, P.: Microstructure and High Temperature-Mechanical Properties of TiC/Graphene/Ti6Al4V Composite Formed by Laser Powder Bed Fusion. Metals 13, 163(2023).https://doi.org/10.3390/met13010163
35. Cao, M., Wang, C.-j., Deng, K.-k., Nie, K.-b., Liang, W., Wu, Y.-c.: Effect of interface on mechanical properties and formability of Ti/Al/Ti laminated composites. J. Mater. Res. Technol. 14, 1655 – 69(2021).https://doi.org/10.1016/j.jmrt.2021.07.021
36. Jafari, R., Eghbali, B., Adhami, M.: Influence of annealing on the microstructure and mechanical properties of Ti/Al and Ti/Al/Nb laminated composites. Mater. Chem. Phys. 213, 313 – 23(2018).https://doi.org/10.1016/j.matchemphys.2018.04.001
37. Yu, H., Li, W., Tan, Y., Tan, Y.: The Effect of Annealing on the Microstructure and Properties of Ultralow-Temperature Rolled Mg – 2Y – 0.6Nd – 0.6Zr Alloy. Metals 11, 315(2021).https://doi.org/10.3390/met11020315
38. Tian, N., Yuan, F., Duan, C., Liu, K., Wang, G., Zhao, G., Zuo, L.: Prediction of the Work-Hardening Exponent for 3104 Aluminum Sheets with Different Grain Sizes. Materials 12, 2368(2019).https://doi.org/10.3390/ma12152368
39. Sun, W., Zhang, R., Cui, N., Zhang, S., Xu, T., Wang, X., Kong, F.: Texture evolution and mechanical properties of Ti-TiAl laminated composite at different rolling temperatures. J. Alloys Compd. 1036, 181858(2025).https://doi.org/10.1016/j.jallcom.2025.181858
40. Boonruang, C., Theppawong, A.: Impact property of TiAl3–Ti laminated composite fabricated from metallic sandwich. Compos. Struct. 229, 111379(2019).https://doi.org/10.1016/j.compstruct.2019.111379